Available online at www.sciencedirect.com

ScienceDirect

Energy Procedia 114 (2017) 3202 – 3209

Energy Procedia

13th International Conference on Greenhouse Gas Control Technologies, GHGT-13, 14-18 November 2016, Lausanne, Switzerland

Coupled thermo-hydro-mechanical effects on caprock stability during carbon dioxide injection

Chao Li*, Lyesse Laloui

Laboratory of soil mechanics - Chair "Gaz naturel" Petrosvibri, Swiss Federal Institute of Technology, EPFL, Lausanne, Switzerland

Abstract

This study presents a numerical investigation of the effects of coupled material properties on the caprock stability. A thermo-hydro-mechanical framework is proposed in order to reproduce the physical processes. The results indicate that for a given geometrical configuration and a given temperature difference between injected CO_2 and reservoir, the potential for the caprock failure may increase or decrease. This contradictory behaviour mainly depends on the combination of the thermal-hydro-mechanical parameters, i.e., thermal expansion coefficient, stiffness and the Biot coefficient. Therefore, the coupled effects of material properties on the caprock stability should be addressed in a combined way for low-temperature CO_2 injection problems.
© 2017 The Authors. Published by Elsevier Ltd. This is an open access article under the CC BY-NC-ND license (http://creativecommons.org/licenses/by-nc-nd/4.0/).
Peer-review under responsibility of the organizing committee of GHGT-13.
Keywords: CO_2 injection; thermo-hydro-mechanical coupling; finite element method; multiphase flow

1. Introduction

The storage of CO_2 in geologic reservoirs, particularly those in deep aquifers, has become a mitigation method used to reduce the impact of CO_2 and the greenhouse effect [1]. There are currently several on-going large-scale projects for CO_2 storage in deep aquifers, such as the In Salah CO_2 storage site in Algeria. The aquifer is usually overlaid with a nearly impermeable caprock which is primary for preventing CO_2 from leakage. Therefore, the caprock stability is a primary concern, which is also the objective of the current investigation.

* Corresponding author. Tel.: +41-21-6932810
E-mail address: chao.li@epfl.ch

1876-6102 © 2017 The Authors. Published by Elsevier Ltd. This is an open access article under the CC BY-NC-ND license (http://creativecommons.org/licenses/by-nc-nd/4.0/).
Peer-review under responsibility of the organizing committee of GHGT-13.
doi:10.1016/j.egypro.2017.03.1683

The hydromechanical (HM) coupled phenomena involved in the CO_2 injection problems have received particular attention. A large volume of CO_2 injection results in the accumulation of overpressure [2]. This overpressure perturbs rapidly the stress field upon injection within the aquifer and extends to the caprock. In addition, the injection temperature is usually lower than that of the aquifer [3], which contracts rocks and reduces stresses if constrained. The two effects may be counterbalanced or superposed depending on the particular configuration of the problem, which deems a fully coupled thermal-hydro-mechanical (THM) investigation [4]. Current literature shows that the low-temperature injection may cause a reduction of compressive stress or even induce tensile stress in the caprock [5], whereas an improvement of the caprock stability has nevertheless been concluded by [6]. This has motivated this study to achieve a unique conclusion whether the failure potential will be attained when the caprock is subjected to a lower temperature under different scenarios. In the scenarios, two key THM coupled properties of rocks are investigated: the HM coupled property, the Biot coefficient, and the thermal-mechanical property, the thermal expansion coefficient. Also, regarding the particular geometrical configuration of CO_2 injection problems (caprock overlying aquifer), material properties combination of caprock and aquifer are believed to affect the response regimes and may also provide an explanation to the aforementioned contradictory conclusions.

The objective of this paper is to fulfil these gaps such that a more rigorous conclusion can be achieved when assessing the caprock stability under low-temperature CO_2 injection. We firstly introduce a CO_2 injection problem in a normal faulting system where essential physical processes are described. The THM fully coupled theoretical formulation is then presented. Next, the coupled effect of the Biot coefficients of both caprock and aquifer, and the caprock's thermal expansion coefficient are investigated, which has to our knowledge not yet been appropriately addressed. These properties are studied from geomechanical and geometrical points of view. The geomechanical point of view is to couple the investigation with parameters such as Young's modulus to achieve more systematic insights. Moreover, the objective from the geometrical point of view is to present the results on caprock stability under the influence of the aquifer's behaviour. Although numerical efforts place a burden on the feasibility of the material properties' sensitivity computations, study cases are carefully chosen to be realistic and to allow to extract novel quantitative information on the effect of the coupled properties on the caprock stability.

2. Thermo-hydro-mechanical formulation of multiphase flows in a deformable media

The compositional approach is employed for this study, as implemented for water and perfect gas by (Collin, 2003) in the finite element code Lagamine. This approach brings the advantage of writing the mass balance equation for two-phase fluids in a straightforward manner. Based on this, we improve the current code with supercritical fluid properties, including terms for storage of both water and CO_2 in supercritical liquid, liquid and gaseous form, the advective flow of both fluids, and non-advective flow of dissolved CO_2 in the water. The THM formulation is described in [4]. Hereafter the THM governing equations are briefly recalled: the mass balance equations (Eq. 1 & Eq. 2), the energy balance equation Eq. 3 and the momentum balance equation Eq. 4.

$$\frac{\partial\left(nS_w\rho_w\right)}{\partial t}+\mathbf{div}\left(\rho_w\mathbf{q}_w\right)=0 \quad \left(\text{mass balance of water}\right) \tag{1}$$

$$\begin{aligned}&\frac{\partial\left(n\left(1-S_w\right)\rho_c\right)}{\partial t}+\mathbf{div}\left(\rho_c\mathbf{q}_c\right)+\\&\frac{\partial\left(nS_w\rho_{dc}\right)}{\partial t}+\mathbf{div}\left(\rho_{dc}\mathbf{q}_w\right)+\mathbf{div}\left(\mathbf{i}_{dc}\right)=0 \quad \left(\text{mass balance of } CO_2\right)\end{aligned} \tag{2}$$

$$\frac{\partial H}{\partial t}+\mathbf{div}\left(\mathbf{\Gamma}\right)+\mathbf{div}\left(\mathbf{f}_\mathbf{T}\right)=0 \quad \left(\text{energy balance}\right) \tag{3}$$

$$\mathbf{div}\left(\boldsymbol{\sigma}\right)+\left[\left(1-n\right)\rho_s+nS_w\rho_w+n\left(1-S_w\right)\rho_c\right]\mathbf{g}=0 \quad \left(\text{momentum balance}\right) \tag{4}$$

where $\boldsymbol{\sigma}$ is the Cauchy stress tensor, **g** the gravity acceleration vector, and *n* the porosity of the medium. ρ_w the densities of water, and ρ_c the density of different phase of CO_2 calculated from Peng and Robinson Equation of State [7]. S_w is the water saturation. ρ_{dc} represents the mass fraction of CO_2 dissolved in water and it is obtained through extended Henry law with CO_2 fugacity [4].

Among these terms, the liquid water flow $\mathbf{q}_w$ and supercritical/liquid CO_2 flow $\mathbf{q}_c$ are governed by the generalized Darcy's law:

$$\mathbf{q}_{w,c} = -\frac{\mathbf{k}k_{rw,rc}}{\mu_{w,c}}\left[\mathbf{grad}\left(p_{w,c}\right) + \rho_{w,c}\mathbf{g}\right] \tag{5}$$

where **k** is the intrinsic permeability and k_{rw}, k_{rc} are water and CO_2 relative permeability, which are material dependent parameters. μ_w is the dynamic viscosity of water and μ_c is the dynamic viscosity of CO_2.

A power law is used to describe the relative permeability as shown in Table. 1. A van Genuchten function [8] is to characterise the retention behaviour of rocks:

$$S_w = \left(1 + \left(\left(p_c - p_w\right)/P_r\right)^{1/(1-m)}\right)^{-m} \tag{6}$$

where m and P_r are a material parameter and a reference pressure, CKW and CKC are material parameters.

The Fick's law governs the CO2 diffusion in water:

$$\mathbf{i}_{dc} = -nS_w\tau D_c\rho_w\mathbf{grad}\left(\frac{\rho_{dc}}{\rho_w}\right) \tag{7}$$

in which D_c is the diffusion coefficient of the dissolved CO_2 in the water phase and τ is the tortuosity of the porous media.

The heat transfer is composed of the heat conduction $\boldsymbol{\Gamma}$ and the convection $\mathbf{f_T}$. The mixture enthalpy *H* is defined as the sum of the heat of each constituent with neglect of the contribution of dissolved CO_2 in the water:

$$H = \left(1-n\right)\rho_s c_{p,s}\left(T - T_0\right) + nS_r\rho_w c_{p,w}\left(T - T_0\right) + n\left(1 - S_r\right)\rho_c h_c \tag{8}$$

where $c_{p,\alpha}$ is the heat capacity of the component α. The term h_c corresponds to the specific enthalpy of CO_2 which is temperature and pressure dependent. It is determined through the fundamental thermodynamics relationship by integrating the Peng and Robinson EOS [4].

The heat transfer is governed by the heat conduction and convection:

$$\begin{aligned}\boldsymbol{\Gamma} + \mathbf{f_T} = &-\left(nS_w\lambda_w + n\left(1-S_w\right)\lambda_C + \left(1-n\right)\lambda_S\right)\mathbf{grad}T \\ &+ c_{p,w}\left(T - T_0\right)\rho_w\mathbf{q}_w + h_c\rho_c\mathbf{q}_c\end{aligned} \tag{9}$$

The total stress is decomposed into the generalized effective stress tensor $\boldsymbol{\sigma}'$ and and fluid pressures:

$$\boldsymbol{\sigma} = \boldsymbol{\sigma}' + b\left(S_w p_w + \left(1 - S_w\right)p_c\right)\mathbf{I} \tag{10}$$

where **I** is the identity matrix**.** An important ingredient that contributes to the thermo-mechanical coupling is accounted for the definition of strain, due to the phenomenon of thermal expansion. The following description of thermo-elastic strains is used:

$$d\boldsymbol{\varepsilon} = \mathbf{E}^{-1}d\boldsymbol{\sigma}' - \alpha_s\mathbf{I}dT \tag{11}$$

where $d\boldsymbol{\varepsilon}$ is the total strain tensor increment, **E** the linear elastic tensor, α_s the thermal expansion coefficient.

3. Conceptual model characteristics

Fig. 1 presents the geometry and the boundary conditions of the model under investigation. The model consists of three essential geology stratum involved in the CO_2 storage problem, sealing caprock, storage aquifer, and underburden rock, which are porous media.

To understand the coupling effect of the overpressure and the temperature on the deformable porous media mechanics, it is necessary to define the appropriate conditions that are encountered in a CO_2 storage project. The injection of CO_2 is modelled as a prescribed CO_2 mass flow at one million tonnes per year through a vertical well along the thickness of the aquifer in a normal faulting system. The initial temperature of the reservoir is set as 330K. The injection temperature is imposed at 300K. The aquifer is considered to be water saturated before the injection and acts as a host medium for CO_2. The caprock is nearly impermeable to prevent CO_2 from leakage. A constantly distributed stress of 13.5MPa is applied along the top of the caprock, being equivalent to the overburden's dead load. The displacement on the right-hand side and bottom of the model is constrained in the perpendicular direction.

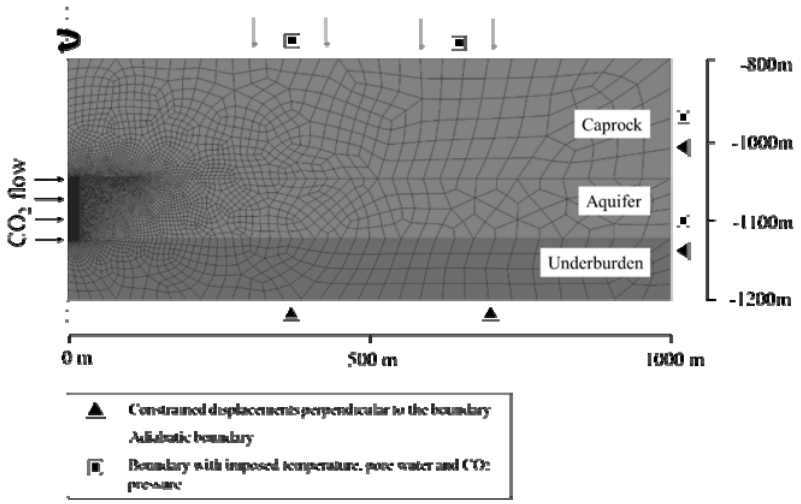

Fig. 1. Geometry, mesh and boundary condition of the model

The sealing caprock usually involves very low permeability and porosity while the aquifer is much more porous, whereupon we consider clayey shale as caprock, and sandstone as storage rock as in most on-going CO_2 storage project [9]. The fluid thermodynamic properties and geomaterial parameters are taken as averaged values from [10]. The model consists of 8723 quadrilateral elements and is run as an axisymmetric model. The initial stress equilibrium is obtained between the application of the body force and the lithostatic stress along the top of the caprock. The lateral earth pressure ratio is taken as $K0$=0.6 as for a normal stress faulting system.

Table. 1. Material parameters for the reference model

Thermal parameters	Symbol	Unit	Seal	Aquifer	Underburden
Saturated thermal conductivity	λ_s	W/(m.K)	1.50	2.50	1.50
Water thermal conductivity	λ_w	W/(m.K)	0.67	0.67	0.67
CO_2 thermal conductivity	λ_a	W/(m.K)	0.08	0.08	0.08
Solid specific heat capacity	$c_{p,s}$	J/(kg.K)	950	850	950
Water specific heat capacity	$c_{p,w}$	J/(kg.K)	4183	4183	4183
Solid thermal expansion coef.	α_s	K^{-1}	1×10^{-5}	1×10^{-5}	1.5×10^{-5}
Water thermal expansion coef.	β_w	K^{-1}	4.5×10^{-5}	4.5×10^{-5}	4.5×10^{-5}
Flow parameters					
Intrinsic permeability	k_{int}	m^2	1×10^{-18}	1×10^{-13}	1×10^{-18}
CO_2 relative permeability	k_{rc}	-	S_c^6	S_c^3	S_c^6

Water relative permeability	k_{rw}	-	S_w^6	S_w^3	S_w^6
Van Genuchten parameter	m	-	0.80	0.50	0.80
Van Genuchten parameter	P_r	MPa	0.60	0.02	0.60
Initial porosity	n_0	-	0.01	0.10	0.01
Tortuosity	τ	-	0.50	0.50	0.50
Other parameters					
Solid specific mass	ρ_s	kg/m^3	2700	2400	2700
Water specific mass	ρ_w	kg/m^3	1000	1000	1000
Mechanical parameters					
Young modulus	E	GPa	5.0	2.5	5.0
Poisson ratio	ν	-	0.30	0.30	0.30
Initial stress factor	*K0*	-	0.60	0.60	0.60

4. Coupled analysis of CO_2 injection induced stress variation in the caprock

4.1. Thermo-mechanical coupling

The thermal expansion coefficient governs the shrinkage level of the rocks upon cooling, of which few literature addresses this aspect for CO_2 problems, a value of unity is usually considered in the studies. Cooling induced stress reduction is sensitive to the thermal expansion coefficient of the material. Experimental investigations show that the coefficient differs from unity and is in the range of *1.0E-5 to 2.0E-5* [11,12]. The quantitative influence of the coefficient is interesting to be investigated.

Fig. 2 shows graphs of the horizontal stress reduction and displacement for three thermal expansion coefficients of the caprock $\alpha_c = \alpha_a$, $1.5\alpha_a$ and $2\alpha_a$ with α_a *=1.0E-5* in three cases. For the sake of clarity, as its overall behaviour varies slightly in the later period of injection, the horizontal stress variation is only shown at 100 days whereas the displacement is shown at 4 times of the first year. Fig. 2d-f show that the horizontal displacement increases very slightly in the negative direction with an increase in the thermal expansion coefficient. The displacement is still very constrained as mentioned previously. Consequently, the increase in the thermal expansion coefficient can only trigger a severe reduction of stress under such deformation constrained condition. The magnitude of this effective stress reduction is proportional to the value of thermal expansion coefficient for a given stiffness of rock. Note that for the case where thermal expansion coefficients of both caprock and aquifer are equal, $\alpha_c = \alpha_a$, the horizontal stress drops more in the caprock than in the aquifer because of caprock possessing a twice higher stiffness as the aquifer.

Caprock's stiffness is thus investigated. As shown in the Fig. 3, three stiffness of the caprock $E_c = 1, 2$ and 5 GPa are considered for a setup of thermal expansion coefficient $\alpha_c = 1.5\ \alpha_a$, $E_a = 2.5GPa$ for the aquifer and $\upsilon = 0.3$ for both caprock and aquifer. The results are shown for 100 days and 300 days after the beginning of injection, where the temperature at interface has already reached the injection temperature. For all three cases, the vertical effective stress undergoes a similar magnitude of reduction, which is not significantly influenced by variations in Young's modulus, whereas the Young's modulus has a major impact on the horizontal effective stress reduction. For the lowest value of $E_c = 1GPa$, the ratio $R = \frac{E_c\alpha_c}{1-2\upsilon} \Big/ \frac{E_a\alpha_a}{1-2\upsilon}$ between the caprock and aquifer is small as $R = 0.6$. The decreased horizontal effective stress upon cooling is therefore lower in the caprock than that in the aquifer. The decrease in the vertical effective stress is higher than the horizontal one with this combination inside the caprock. In the case that the stiffness of the caprock is equal to $E_c = 2GPa$, shown in Fig. 3b, that is though smaller than that of the aquifer, $\frac{E\alpha}{1-2\upsilon}$ of the caprock is slightly higher due to a higher thermal expansion coefficient, leading to $R = 1.2$. The decrease in horizontal effective stress is thereby lightly more in the caprock than that in the aquifer, which is less than the effective stress reduction of the vertical one at the interface caprock-

aquifer. As long as the ratio is high as $R = 3$ as illustrated in Fig. 3c, the horizontal stress has a major reduction and is higher than the decrease in the vertical effective stress.

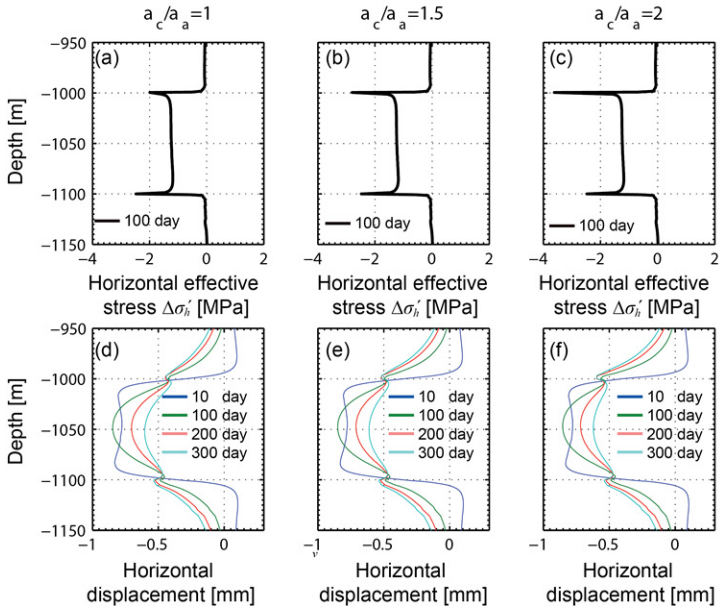

Fig. 2. Effect of the thermal expansion coefficient of the caprock on the horizontal stress variations and the horizontal displacement at 5 metres away from the injection well.

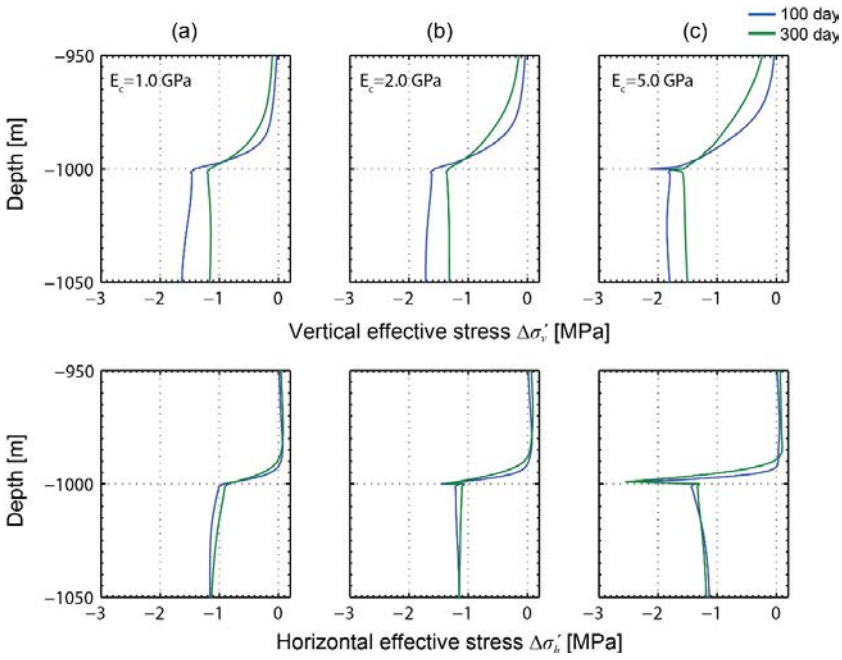

Fig. 3. Effect of the caprock's Young modulus on the vertical and horizontal effective stress variations at 5 metres away from the injection well.

4.2. Hydro-mechanical coupling

The Biot coefficient b governs the percentage of stress reduction which is caused by the overpressure, defined as $= 1 - K_m/K_s$, K_m is the bulk modulus of the porous matrix and K_s the bulk modulus of the solid matrix. For a soft and unconsolidated rock $b = 1$; for a stiff rock $0.5 < b < 1$. The Biot coefficient is assumed to be 1 in current numerical studies [13], but the coefficient usually differs from unit for sandstones from experimental studies [14,15]. Noted that a Biot coefficient of 0.5 can reduce the overpressure effect by a half. Recent study has shown that a very low porous shale has a Biot coefficient close to 0.9 [16].

Fig. 4 illustrates the effect of the Biot coefficient of the aquifer on the vertical effective stress variation $\Delta\sigma_v'$ and vertical displacement. Comparison between the graphs in Fig. 4a and 4c reveals that the Biot coefficient has moderate influence on the vertical displacement and minor influence on the stress reduction. The effect of the overpressure on the effective stress is reduced with a lower value of the Biot coefficient, whereupon the aquifer undergoes a smaller order of magnitude of the expansion. The displacement reduces 30% at 10 days when the Biot coefficient of the aquifer turns 1.0 to 0.6. Accordingly, the caprock undergoes the same reduction because of the displacement continuity. Since the initial expansion driven by overpressure is reduced with a lower Biot coefficient while subsequent cooling remains at dominant impact on deformation, a negative vertical displacement is eventually observed at 300 days. This suggests that the caprock settlement will be induced by a long-term cooling when the hydromechanical coupling term becomes weak. The results in Fig. 4b-d demonstrate that the consideration of caprock's Biot coefficient has a negligible effect on the caprock deformation. The level of displacement in the lower portion of the caprock is essentially controlled by the expansion of the aquifer, which implies that it is primarily influenced by the consideration of the Biot's coefficient of the aquifer. Subsequent reduce of vertical stress is solely affected by cooling not by the hydromechanical coupling.

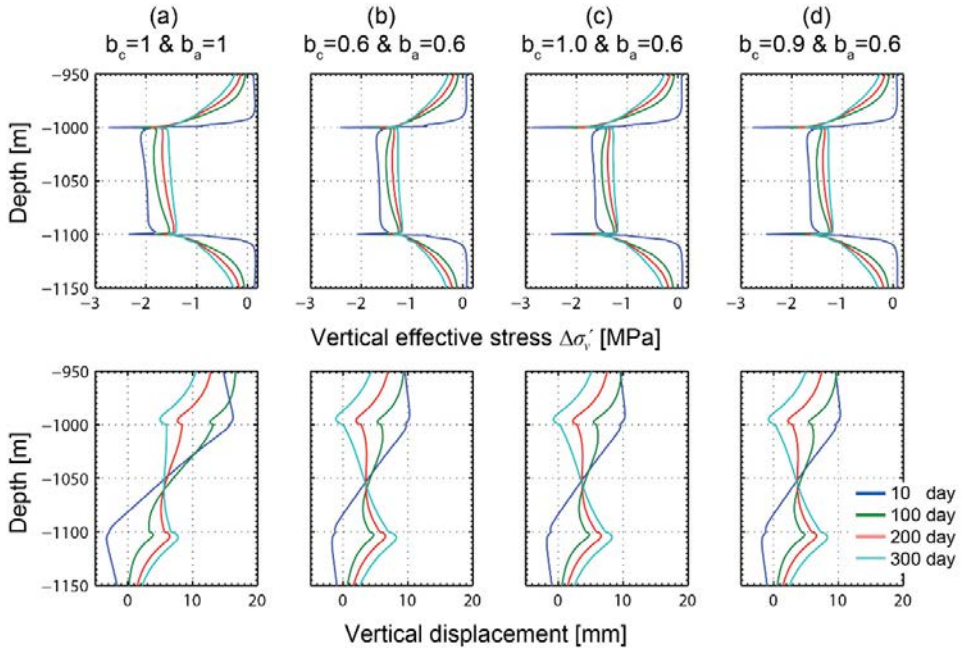

Fig. 4 Effect of the Biot coefficient on the vertical effect stress variations and vertical displacement at 5 metres away from the injection well.

Conclusions

The study has revealed a high importance of the low-temperature injection in relation to the stress variation caprock stability, which is influencing by the coupled nature of the thermal, hydraulic, and mechanical phenomena

that occur. The results are presented in terms of the different thermal-elastic parameter ratios $R = \frac{E_c\alpha_c}{1-2\upsilon} / \frac{E_a\alpha_a}{1-2\upsilon}$, showing that for a given temperature decrease, the injection may increase caprock stability when $R<1$ while decrease the stability when $R > 4$ (a stiffer caprock with a higher thermal expansion coefficient). The present simulations are consistent with the earlier predictions, emphasizing in addition that the caprock with a higher ratio R is in a high potential towards the failure, deteriorating the mechanical stability.

The present results also complement earlier studies, extending them in the geophysical range of conditions where the hydro-mechanical parameter are substantially valid in practice. The consideration of the aquifer's Biot coefficient is essential for properly estimating the expansion of the aquifer and eventually the surface movement. However, the consideration of the coefficient of Biot for caprock doesn't have an influence on the results because no HM coupling processes occur inside the caprock in this study. Nevertheless, it is necessary to be investigated if a higher permeable caprock is involved in the problem since the overpressure may penetrate, leading to the occurrence of HM processes within the caprock.

The high degree of coupled complex phenomena observed in this study leads to paradoxical results such that a change of thermally coupled parameter combination (Young's modulus and thermal expansion coefficient) may reduce or improve the caprock stability. For this reason, the effects presented with a set of parameters are very risky to be extrapolated to another situation in which the materials may have quite different properties, the environmental loading and the geometrical configurations are different as well.

References

[1] Bryant E. Climate Process and Change. Cambridge, UK: Cambridge University Press, 1997; 1997.

[2] Li C, Barès P, Laloui L. A hydromechanical approach to assess CO2 injection-induced surface uplift and caprock deflection. Geomech Energy Environ 2015;4:51–60. doi:10.1016/j.gete.2015.06.002.

[3] Bissell RC, Vasco DW, Atbi M, Hamdani M, Okwelegbe M, Goldwater MH. A full field simulation of the in Salah gas production and CO2 storage project using a coupled geo-mechanical and thermal fluid flow simulator. Energy Procedia 2011;4:3290–7. doi:10.1016/j.egypro.2011.02.249.

[4] Li C, Laloui L. Coupled multiphase thermo-hydro-mechanical analysis of supercritical CO2 injection: Benchmark for the In Salah surface uplift problem. Int J Greenh Gas Control 2016;51:394–408. doi:10.1016/j.ijggc.2016.05.025.

[5] Preisig M, Prévost JH. Fully coupled simulation of fluid injection into geomaterials with focus on nonlinear near-well behavior. Int J Numer Anal Methods Geomech 2012;36:1023–40. doi:10.1002/nag.1039.

[6] Vilarrasa V, Olivella S, Carrera J, Rutqvist J. Long-term impacts of cold CO2 injection on the caprock integrity. Int J Greenh Gas Control 2014;24:1–13. doi:10.1016/j.ijggc.2014.02.016.

[7] Peng D-Y, Robinson DB. A New Two-Constant Equation of State. Ind Eng Chem Fundam 1976;15:59–64. doi:10.1021/i160057a011.

[8] van Genuchten MT. A Closed-form Equation for Predicting the Hydraulic Conductivity of Unsaturated Soils. Soil Sci Soc Am J 1980;44:892. doi:10.2136/sssaj1980.03615995004400050002x.

[9] Metz B, Davidson O, de Coninck H, Loos M, Meyer L. IPCC Special Report on Carbon Dioxide Capture and Storage. 2005. doi:10.1002/anie.201000431.

[10] Rutqvist J, Tsang C-F. A study of caprock hydromechanical changes associated with CO 2 -injection into a brine formation. Environ Geol 2002;42:296–305. doi:10.1007/s00254-001-0499-2.

[11] Jobmann M, Polster M. The response of Opalinus clay due to heating: A combined analysis of in situ measurements, laboratory investigations and numerical calculations. Phys Chem Earth, Parts A/B/C 2007;32:929–36. doi:10.1016/j.pce.2006.03.014.

[12] Gilliam TM, Morgan TM. Shale: Measurement of Thermal Properties (No. ORNL/TM-10499). Oak Ridge National Lab., TN (USA). Oak Ridge, Tennessee: 1987.

[13] Orlic B. Some geomechanical aspects of geological CO2 sequestration. KSCE J Civ Eng 2009;13:225–32. doi:10.1007/s12205-009-0225-2.

[14] Vidal-Gilbert S, Tenthorey E, Dewhurst D, Ennis-King J, Van Ruth P, Hillis R. Geomechanical analysis of the Naylor Field, Otway Basin, Australia: Implications for CO2 injection and storage. Int J Greenh Gas Control 2010;4:827–39. doi:10.1016/j.ijggc.2010.06.001.

[15] Nur A, Byerlee JD. An exact effective stress law for elastic deformation of rock with fluids. J Geophys Res 1971;76:6414. doi:10.1029/JB076i026p06414.

[16] Ferrari A, Favero V, Laloui L. One-dimensional compression and consolidation of shales. Int J Rock Mech Min Sci 2016;88:286–300. doi:10.1016/j.ijrmms.2016.07.030.